Two-photon quantum state engineering in nonlinear photonic nanowires

Dongpeng Kang,[1,2,*] Arthur Pang,[1] Yuxiang Zhao,[1] and Amr S. Helmy[1,2]

[1]*The Edward S. Rogers Department of Electrical and Computer Engineering, University of Toronto, 10 King's College Road, Toronto, Ontario M5S 3G4, Canada*
[2]*Institute for Optical Sciences, University of Toronto, 60 St. George Street, Toronto, Ontario M5S 3G4, Canada*
**Corresponding author: dongpeng.kang@mail.utoronto.ca*

Received February 27, 2014; revised April 24, 2014; accepted May 10, 2014; posted May 12, 2014 (Doc. ID 206905); published June 19, 2014

We propose and analyze a generic technique to engineer the two-photon quantum state generated by spontaneous parametric downconversion (SPDC) in nonlinear photonic nanowires using any suitable material system. Through dispersion engineering in nanowires, the group velocity of each photon involved in the SPDC process can be tuned such that pure heralded single photons or maximally polarization entangled photons can be directly generated on a chip. Implementations in III–V semiconductor and ferroelectric waveguides demonstrate minimal frequency correlations with Schmidt numbers of ∼1 for heralded single photons, and maximal entanglement with concurrences of ∼1 for polarization entangled photons. © 2014 Optical Society of America

OCIS codes: (130.3120) Integrated optics devices; (190.4390) Nonlinear optics, integrated optics; (230.4320) Nonlinear optical devices; (270.5585) Quantum information and processing.
http://dx.doi.org/10.1364/JOSAB.31.001581

1. INTRODUCTION

Quantum states of photons are indispensable sources for various applications in the fields of quantum optics and quantum information processing, such as quantum key distribution and quantum computing [1–3]. The generation and engineering of quantum states of photons has always been a task of high priority [4,5]. These quantum states include, but are not limited to, entangled photons and single photons.

Entangled photon pairs are conventionally generated via the nonlinear optical process of spontaneous parametric downconversion (SPDC), in which a pump photon is annihilated, and a pair of photons called signal and idler are created [6]. The photons making up a downconverted pair can be engineered such that they are entangled in one or more degrees of freedom, such as polarization, spatial mode, and frequency. In the most studied case of polarization entanglement, photons in different pairs need to be indistinguishable in every degree of freedom, except for polarization [5]. This usually means that the spectral distinguishability needs to be removed by spectral filtering, and the temporal distinguishability removed by path compensation. Other techniques such as using interferometers have also been developed to produce polarization entangled photons [7,8].

On the other hand, single photons could ideally be generated by quantum emitters such as quantum dots, which emit identical photons one at a time [9,10]. A more readily available approach to generate single photons is to use photon pairs. In this method, the detection of one photon (the heralding photon) in a pair heralds the arrival of its twin (the heralded single photon). As such, paired photons should be uncorrelated in frequency, so that the heralded single photon is in a pure quantum state. This conventionally requires spectral filtering to remove the spectral correlation. Instead, pure single photons can be directly generated without filtering via a technique called group velocity matching; this option, however, is limited and is dictated by the choice of material and photon wavelengths in nonlinear crystals [5,11,12].

Meanwhile, driven by the need for highly efficient, compact sources of photon pairs required by any practical quantum information processing system, nonlinear waveguides have attracted a lot of research in the past decade [13]. These include $\chi^{(2)}$ waveguides using SPDC [14–16] and $\chi^{(3)}$ waveguides using spontaneous four-wave mixing (SFWM) [17–20]. Due to the tight confinement of waveguide modes and the effective long interacting length, the generation efficiency can be increased by a few orders of magnitude compared to their bulk crystal counterparts.

In addition, practical applications employing such sources require them to be mobile, robust, and alignment-free, which is still an active topic of research. To this end, it is advantageous to generate a particular quantum state of photons directly on a chip without using extra components. For example, in periodically poled potassium titanyl phosphate (PPKTP) waveguides, pure single photons can be produced directly in certain wavelengths without spectral filtering, thanks to the natural dispersion properties of this material system, which are able to satisfy the group velocity matching conditions required [21]. More importantly, dispersion engineering of waveguide devices provides a powerful way to generate photon pairs with properties not naturally allowed by material dispersions. For example, pure single-photon generation by group velocity matching can be accomplished by engineering a Bragg reflection waveguide [22], and a polarization entangled photon can be directly produced by engineering the waveguide modal birefringence [23] or the group birefringence [24]. Recently, it was proposed that mode and

polarization hyperentangled photons can be generated on a chip through waveguide engineering [25].

Among all waveguide sources, those with subwavelength confinement, or photonic nanowires, have been of particular interest. On the one hand, the tight confinement of light could further increase the conversion efficiency of the nonlinear process compared to weakly guided waveguides [26,27]. This is in part because in photonic nanowires the waveguide dispersion could outweigh the material dispersion, allowing for drastic control over the modal dispersion properties that are required for phase matching [27,28] or two-photon state engineering [29]. Most photon pair sources in photonic nanowires have been demonstrated using SFWM in silica [30,31] and silicon-based materials [32–35] due to the well-developed fabrication technology and the relaxed requirement on phase matching. Sources that use SPDC in $\chi^{(2)}$ photonic nanowires are equally important due to the potentially incomparable efficiencies [26] in a large range of $\chi^{(2)}$ materials and have not been demonstrated to date.

In this work, we demonstrate how tailoring the waveguide dispersion in photonic nanowires provides a simple yet powerful technique to engineer the two-photon quantum state in $\chi^{(2)}$ materials. Via dispersion engineering, pure heralded single photons or maximally polarization entangled photons can be generated directly on-chip without the need for any other components. This technique is generic, and does not require complex nanoscale patterns to be defined. It can be used to generate the aimed quantum states on a chip in any material system.

This paper is organized as follows: in Section 2, we review the quantum mechanical treatment of SPDC in nonlinear waveguides and present the requirements for generating pure single photons and maximally polarization entangled photons. In Section 3, we show how these requirements could all be satisfied by dispersion engineering in photonic nanowires. Section 4 presents the analyses of design examples based on III–V semiconductor $Al_xGa_{1-x}As$ and ferroelectric lithium niobate, respectively, where the device performance is numerically evaluated. Section 5 summarizes the findings.

2. FORMALISM

A. Spontaneous Parametric Downconversion in Waveguides

The quantum state of the photons generated by SPDC can be conventionally obtained using the time-dependent perturbation theory in the interaction picture [11,36], or, equivalently, using the backward Heisenberg picture approach [37,38]. Following [37,38], the Schrödinger picture nonlinear Hamiltonian is given by

$$H=\sum_{\alpha,\beta,\gamma}\int \mathrm{d}\omega_1\mathrm{d}\omega_2\mathrm{d}\omega S_{\alpha\beta\gamma}(\omega_1,\omega_2,\omega)a^{d\dagger}_{\alpha\omega_1}a^{d\dagger}_{\beta\omega_2}a^{p}_{\gamma\omega}+\mathrm{H.c.}, \quad (1)$$

where the Greek subscripts denote the polarization, and $a^{p}_{\sigma\omega}$ and $a^{d}_{\sigma\omega}$ are the boson mode operators for the pump and downconverted photons, respectively, associated with angular frequency ω and polarization σ. They satisfy commutation relation $[a^{m}_{\sigma\omega},a^{m'\dagger}_{\sigma'\omega'}]=\delta_{mm'}\delta_{\sigma\sigma'}\delta(\omega-\omega')$ for $m,m'=p,d$. $S_{\alpha\beta\gamma}(\omega_1,\omega_2,\omega)$ is a function determined by the phase matching condition, modal overlap, material nonlinear coefficient, pump pulse spectrum, etc. In the following, we will assume the pump has single polarization and thus omit the summation over γ. The asymptotic-out quantum state of the generated photons in the limit of low probability of pair production per pump pulse ($|\nu|^2\ll 1$) can be written as $|\Psi_{\mathrm{gen}}\rangle\approx|vac\rangle+\nu|II\rangle$, where

$$|II\rangle=\frac{1}{\sqrt{2}}\int \mathrm{d}\omega_1\mathrm{d}\omega_2\sum_{\alpha,\beta}\phi_{\alpha\beta}(\omega_1,\omega_2)a^{d\dagger}_{\alpha}(\omega_1)a^{d\dagger}_{\beta}(\omega_2)|vac\rangle \quad (2)$$

is the normalized two-photon state. The biphoton wave function (BWF) $\phi_{\alpha\beta}(\omega_1,\omega_2)$ at the output facet of the waveguide of length L is

$$\phi_{\alpha\beta}(\omega_1,\omega_2)\propto\phi_P(\omega_1+\omega_2)\mathrm{sinc}\left(\frac{\Delta k_{\alpha\beta}L}{2}\right)\exp\left(-i\frac{\Delta k_{\alpha\beta}L}{2}\right), \quad (3)$$

where $\phi_P(\omega)$ is the pump spectral amplitude at the output facet, $\Delta k_{\alpha\beta}(\omega_1,\omega_2)=k^{p}_{\gamma}(\omega_1+\omega_2)-k^{d}_{\alpha}(\omega_1)-k^{d}_{\beta}(\omega_2)-2\pi/\Lambda$ is the phase matching function in the case that quasi-phase-matching (QPM) [39] is used, and Λ is the first-order QPM grating period. In general, the pump spectral amplitude is taken to be Gaussian, i.e., $\phi_P(\omega)\propto\exp[-(\omega-\omega_p)^2/\Omega^2]$, with a center frequency ω_p and time-domain intensity full width at half-maximum $2\sqrt{2\ln 2}/\Omega$. The propagation constant of each mode around the degenerate PM frequency ω_{m0} ($m=p,d$) can be calculated by

$$k^{m}_{\sigma}(\omega)=k^{m}_{\sigma}(\omega_{m0})+\frac{\omega-\omega_{m0}}{v^{m}_{\sigma}}-\frac{\lambda^2_{m0}}{4\pi c}D^{m}_{\sigma}(\omega-\omega_{m0})^2,$$

where $v^{m}_{\sigma}=d\omega/dk^{m}_{\sigma}|_{\omega_{m0}}$ and $D^{m}_{\sigma}=-(2\pi c/\lambda)d^2k^{m}_{\sigma}/d\omega^2|_{\omega_{m0}}$ are the corresponding group velocity and group velocity dispersion (GVD), respectively, which can be calculated numerically. Normalization of the two-photon state $|II\rangle$ requires $\int\mathrm{d}\omega_1\mathrm{d}\omega_2\sum_{\alpha,\beta}|\phi_{\alpha\beta}(\omega_1,\omega_2)|^2=1$. Therefore, $|\nu|^2$ can be thought of as the probability of pair generation per pump pulse. Note that the BWF is symmetric under exchange of both mode indices and frequencies $\phi_{\alpha\beta}(\omega_1,\omega_2)=\phi_{\beta\alpha}(\omega_2,\omega_1)$, but it does not necessarily possess any additional symmetry, i.e., $\phi_{\alpha\beta}(\omega_1,\omega_2)\neq\phi_{\beta\alpha}(\omega_1,\omega_2)$, $\phi_{\alpha\beta}(\omega_1,\omega_2)\neq\phi_{\alpha\beta}(\omega_2,\omega_1)$.

The property of two-photon quantum state $|II\rangle$ largely depends on the shape of the BWF given by Eq. (3). Thus engineering the two-photon quantum state essentially relies on engineering the shape of the BWF. We will explain this point in detail for the generation of pure single photons and polarization entangled photons in the following subsections.

B. Heralded Pure Single-Photon Generation

When photon pairs are used as single photons, the detection of one photon heralds the existence of the other one (heralded single photon). In the ideal case, the heralded single photon should be in a quantum pure state. This requires that there is no frequency correlation in the BWF, which can be written as [12]

$$\phi_{\alpha\beta}(\omega_1,\omega_2)=\phi_1(\omega_1)\phi_2(\omega_2). \quad (4)$$

In the case of CW or narrow-band pump, the BWF is always anticorrelated in the (ω_1,ω_2) plane. The nature of the correlation is governed by the pump spectral amplitude

$\phi_P(\omega_1+\omega_2)$ in Eq. (3). However, if the pump pulse is sufficiently broad, the shape of the BWF can be largely determined by the shape of the sinc function in Eq. (3). The sinc function in Eq. (3) has its main lobe oriented at an angle of $\tan^{-1}[(1/v_\alpha^d - 1/v_\gamma^p)/(1/v_\gamma^p - 1/v_\beta^d)]$ in the (ω_1,ω_2) plane. In most cases, material dispersion yields $v_\gamma^p < v_{\alpha,\beta}^d$, and the sinc function is largely anticorrelated in the (ω_1,ω_2) plane as well. As a result, the frequency separability required by Eq. (4) can never be satisfied in these cases. In order to achieve frequency separability in the BWF, the group velocities of the pump and the downconverted photons must satisfy [12]

$$v_\alpha^d \le v_\gamma^p \le v_\beta^d, \qquad \text{or} \qquad v_\beta^d \le v_\gamma^p \le v_\alpha^d. \tag{5}$$

These requirements are called group velocity matching. They enable the erasure of the frequency correlation in the BWF by changing the orientation of the sinc function and the bandwidth of the pump in Eq. (3). In one extreme case, if the group velocity of the pump equals that of one of the downconverted photons, i.e., $v_\gamma^p = v_{\alpha,\beta}^d$, the sinc function would be mainly parallel to one of the axes in the (ω_1,ω_2) plane. In such a case, as long as the pump bandwidth is sufficiently broad, the BWF is approximately uncorrelated in frequency. In another extreme case, if $2/v_\gamma^p = 1/v_\alpha^d + 1/v_\beta^d$, the sinc function would be perpendicular to the pump spectrum function in Eq. (3). This allows us to switch between anticorrelated, uncorrelated, and correlated photon pairs by varying the pump bandwidth (see, e.g., Ref. [5,22]). In the first extreme case, the signal and idler have different spectra even if they are uncorrelated in frequency, whereas in the latter extreme case, the paired photons can be uncorrelated and indistinguishable.

In most cases, group velocity matching can only be satisfied by choosing appropriate wavelengths for certain materials [12,21]. It can also be achieved by engineering the dispersion of the waveguide spatial modes [22], which enables the generation of pure single photons not naturally allowed by the given materials. The latter method will be used in this work.

To quantify the degree of spectral entanglement of the BWF, we calculate the Schmidt decomposition, which is defined as $\phi_{\alpha\beta}(\omega_1,\omega_2) = \sum_n \sqrt{p_n}\, U_{\alpha n}(\omega_1) V_{\beta n}(\omega_2)$, where p_n are the eigenvalues of the matrix $\rho_{\omega'\omega}^{\alpha\beta} = \int \phi_{\alpha\beta}^*(\omega',\omega'')\phi_{\alpha\beta}(\omega,\omega'')\mathrm{d}\omega''$, with $\sum_n p_n = 1$, and $U_{\alpha n}$, $V_{\beta n}$ are the corresponding Schmidt modes. The degree of entanglement or separability is characterized by the Schmidt number

$$K = \frac{1}{\sum_n p_n^2} \tag{6}$$

with $K = 1$ corresponding to a separable two-photon state and an increasing value of K corresponding to an increase of the degree of entanglement.

C. Polarization Entangled Photon Generation

We now consider the generation of polarization entangled photons. One of the most widely used methods to produce polarization entangled photons from waveguides is via a type-II SPDC process, in which cross-polarized photons are generated in a pair. The two-photon state can be explicitly written as

$$|II\rangle = \frac{1}{\sqrt{2}} \int \mathrm{d}\omega_1 \mathrm{d}\omega_2 [\phi_{HV}(\omega_1,\omega_2)|\omega_1 H;\omega_2 V\rangle + \phi_{VH}(\omega_1,\omega_2)|\omega_1 V;\omega_2 H\rangle], \tag{7}$$

where H, V denote TE and TM polarizations, respectively, and $|\omega_1\alpha;\omega_2\beta\rangle = a_\alpha^{d\dagger}(\omega_1) a_\beta^{d\dagger}(\omega_2)|vac\rangle$. The photons in a pair must be spatially separated. One way to achieve this is to use a 50:50 beamsplitter to split the photons nondeterministically and use postselection, which entails losing half of the photons. An alternative method is to split the photons deterministically using a dichroic mirror. For an ideal dichroic mirror with a splitting frequency of $\omega_0 = \omega_p/2$, the resulting state is given by

$$|II\rangle \propto \int_0^{\omega_0} \mathrm{d}\omega_1 \int_{\omega_0}^{\infty} \mathrm{d}\omega_2 [\phi_{HV}(\omega_1,\omega_2)|\omega_1 H;\omega_2 V\rangle + \phi_{VH}(\omega_1,\omega_2)|\omega_1 V;\omega_2 H\rangle]. \tag{8}$$

For the quantum state given by Eq. (8) to be maximally entangled in polarization, it must be factorizable with respect to the polarization and spectral-temporal degrees of freedom, which requires

$$\phi_{HV}(\omega_1,\omega_2) = \phi_{VH}(\omega_1,\omega_2), \tag{9}$$

or, equivalently,

$$\phi_{HV}(\omega_1,\omega_2) = \phi_{HV}(\omega_2,\omega_1).$$

In this case, it is impossible to discern the polarization of each photon by looking at the spectral and temporal information. However, as mentioned before, Eq. (9) is not satisfied in general.

The asymmetry in the BWF is mainly due to the nonzero group velocity mismatch (GVM) between the downconverted photons $|1/v_\alpha^d - 1/v_\beta^d|$. On the one hand, the GVM causes temporal walk-off between cross-polarized photons, as manifested by the phase of the BWF in Eq. (3). Therefore, the polarizations can be inferred from the arrival times of the two photons. On the other hand, the GVM, combined with the nonnegligible GVDs, causes asymmetry in the joint spectral amplitude $|\phi_{\alpha\beta}(\omega_1,\omega_2)|$, which results in spectral distinguishability [24]. The latter is more obvious in waveguides with large GVD, such as those made of $Al_xGa_{1-x}As$. As a result, generating polarization entangled photons usually relies on the use of off-chip compensation, spectral filtering, or interferometric setups to remove any distinguishing information [6,13].

In order to generate maximally polarization entangled photons directly from the chip, the goal is to produce a two-photon state with a symmetric BWF as indicated by Eq. (9). As demonstrated before, this requirement can be satisfied to a good approximation if the GVM between the downconverted photons is approximately zero [24].

To quantify the degree of polarization entanglement, we can express the density matrix in the polarization subspace by tracing over the frequency degree of freedom, and calculate the concurrence C, an entanglement monotone, as a figure of merit [40,41]. It is calculated by

$$C = 2\left| \int_0^{\omega_0} \mathrm{d}\omega_1 \int_{\omega_0}^{\infty} \mathrm{d}\omega_2 \phi_{HV}(\omega_1,\omega_2)\phi_{VH}^*(\omega_1,\omega_2) \right|, \tag{10}$$

where the normalization condition requires

$$\int_0^{\omega_0} d\omega_1 \int_{\omega_0}^{\infty} d\omega_2 [|\phi_{HV}(\omega_1,\omega_2)|^2 + |\phi_{VH}(\omega_1,\omega_2)|^2] = 1.$$

A maximum concurrence of $C = 1$ indicates maximal polarization entanglement, whereas $C = 0$ represents a separable state.

3. DISPERSION ENGINEERING IN PHOTONIC NANOWIRE WAVEGUIDES

In the previous section, we showed that the generation of pure single photons and polarization entangled photons relies on matching the group velocities of either the pump and the signal or idler, or the signal and idler. In this section we will show that the required dispersion engineering can be achieved in photonic nanowire waveguides. To illustrate this point, we consider the simplest, symmetric, three-layer slab waveguide without loss of generality. In order to include material dispersion, we take the waveguide core as $Al_{0.4}Ga_{0.6}As$, which has a steep, normal material dispersion [42], and assume it is surrounded by air to provide sufficient index contrast. We consider photon pairs being generated in the telecommunication band of 1550 nm with the pump wavelength centered at 775 nm.

For both wavelengths, we calculate the group velocities of the fundamental TE and TM modes as functions of the waveguide core thickness, as shown in Fig. 1. The results show that for a given wavelength, the group velocity of the TM mode is more sensitive to the core thickness than that of the TE mode. Taking 1550 nm for example, for a large core thickness, the group velocities are largely determined by the material dispersion. As the core thickness decreases, the group velocity of the TM mode drops significantly to a minimum when the core thickness is around 280 nm. Further decreasing the core thickness will result in a rapid increase of the TM mode group velocity, as the electric field profile loses confinement and spreads out in the cladding layers. Meanwhile, at the same wavelength, the TE mode group velocity has a similar trend but much smaller change over the range of core thickness.

On the other hand, at the pump wavelength of 775 nm, the group velocities are lower for both polarizations at large core thicknesses due to the material dispersion. In addition, the dependence on the core thickness of each mode is similar to its long wavelength counterpart, but with the "dip" in the group velocity taking place for a smaller core thickness (not shown in Fig. 1). As a result, in the range of relatively large core thickness, both group velocities are less sensitive to the change of core thickness when compared to those at the longer wavelength.

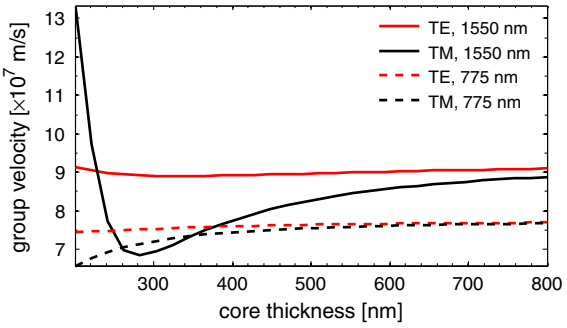

Fig. 1. Dependences of group velocities on the core thickness for a slab waveguide consisting of a core of $Al_{0.4}Ga_{0.6}As$ and claddings of air.

According to Fig. 1, in such a slab waveguide, zero GVM between the TM mode at 1550 nm and the TE or TM modes at 775 nm can be achieved with a core thickness of 378 or 350 nm, respectively. This enables the generation of pure single photons if the pump at a given polarization is downconverted into a pair of photons in TE and TM polarizations. On the other hand, generating maximally polarization entangled photons requires zero GVM between TE and TM modes at 1550 nm. This is satisfied in the weakly guided region with a core thickness of 228 nm.

In the above discussions, we have assumed a large refractive index contrast between the core and the cladding layers. This is necessary for the waveguide dispersion to dominate over the material dispersion, thus allowing for a substantial control on the modal dispersions. In a low index contrast waveguide, the waveguide dispersion could be insufficient to modify the dispersion of a given mode significantly to achieve zero GVM with a mode at half of the wavelength. However, zero GVM between the downconverted photons is still achievable provided the waveguide form birefringence is low.

It should be noted that the different behaviors for the two polarizations arise from the different boundary conditions of the electromagnetic field. Given the electric field orientations of TE and TM modes, one could use the waveguide width in a 2D waveguide to achieve significant control on the group velocity of a TE mode. Combining the effects of the core thickness and the width of a waveguide, greater flexibility on the control of modal dispersions can be achieved. As a result, achieving group velocity matching for the pump and the signal or idler, or the signal and idler, is readily feasible, thus allowing for the generation of pure heralded single photons or maximally polarization entangled photons in a tightly confined nonlinear waveguide.

This technique of two-photon quantum state engineering is not limited to any particular material system. Therefore, it could be applied to generate quantum states of certain properties not naturally supported by the given material.

4. DEVICE DESIGNS

In this section we will consider two illustrative design examples based on III–V semiconductor and ferroelectric materials, respectively, using the strategy described in Section 3. III–V semiconductors are particularly attractive because of the ability of monolithic integration with the pump lasers and other active and passive components, whereas ferroelectric waveguides are so far the most popular waveguide devices used for wavelength conversion and photon pair generation due to their high efficiencies. Specifically, we will consider $Al_xGa_{1-x}As$ for III–V semiconductor and lithium niobate for ferroelectrics to generate photon pairs around 1550 nm. The material refractive index models are taken from [42] and [43], respectively. QPM is utilized in both cases to define the phase matching wavelength.

A. III–V Semiconductor Waveguides

For practical waveguide designs using III–V semiconductor $Al_xGa_{1-x}As$, we assume the core has a thickness of $t_c = 300$ nm and aluminum concentration of $x_c = 0.4$, while the cladding layers have an aluminum concentration of

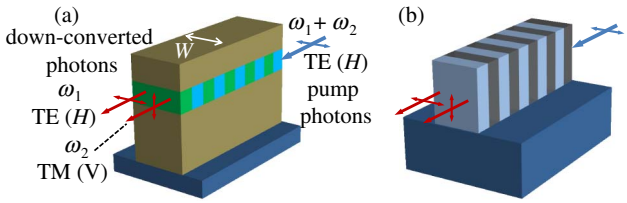

Fig. 2. Schematics of (a) Al_xGa_{1-x} As and (b) lithium niobate waveguides in consideration. Both structures utilize QPM and support type-II SPDC processes.

$x_s = 0.8$. The thicknesses of the upper and lower cladding layers are taken to be 0.5 and 2.2 μm, respectively, which are sufficiently thick to provide vertical mode confinement. The three-layer slab waveguide can be grown on a [001] GaAs substrate, and then etched along the [110] direction to form a ridge waveguide with a width of W. The waveguide supports a type-II SPDC process, in which a TE polarized pump centered at 775 nm is downconverted into a pair of photons near 1550 nm in a TE and TM mode, respectively. The waveguide structure is schematically shown in Fig. 2(a), with the waveguide length taken to be 2 mm.

1. Pure Single Photons

First we consider the generation of pure single photons, which requires the group velocities to satisfy Eq. (5). In a slab waveguide, $v_H^d \approx v_V^d \gg v_H^p$, determined by the material dispersion. Notice in this case, the index contrast between the core and claddings is low ($n_c - n_s \approx 0.1884$ at 1550 nm); thus modifying the core thickness t_c could not bring v_V^d much closer to v_H^p, contrary to the large index contrast case in Fig. (1). However, as mentioned before, we can change the waveguide width W to reduce v_H^d such that $v_H^d = v_H^p$. The dependences of the group velocities on the width are shown in Fig. 3. Comparing with Fig. 1, the group velocities show similar behaviors as the waveguide width decreases, except that the TE mode has a larger change as opposed to the TM mode in Fig. 1.

Figure 3 shows that zero GVM between the downconverted TE mode and the pump TE mode is achieved when $W \approx 0.31$ μm. The corresponding first-order QPM grating period is 1.04 μm.

For this structure, we plot the joint spectral intensity (JSI) $|\phi_{HV}(\omega_1, \omega_2)|^2$ for 500 fs pump pulses, as shown in Fig. 4. The JSI is cigar-shaped and oriented along the axis of the TE photon wavelength, as expected from the group velocity matching

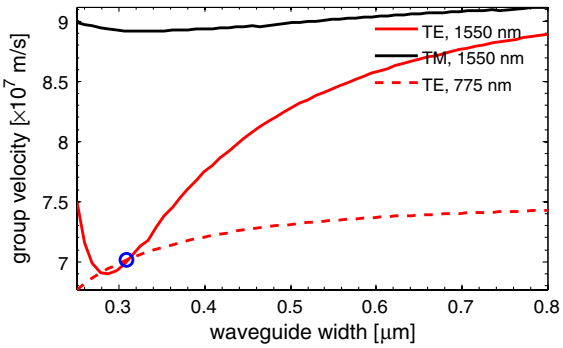

Fig. 3. Dependences of group velocities on the width for an Al_xGa_{1-x} As ridge waveguide.

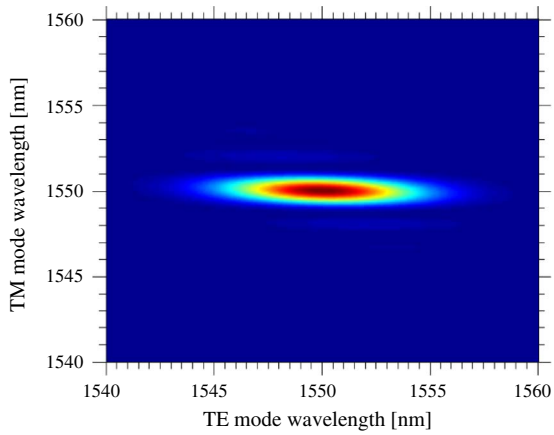

Fig. 4. JSI of the generated photon pairs in an Al_xGa_{1-x} As ridge waveguide using 500 fs pump pulses. The corresponding Schmidt number is 1.05.

condition. The Schmidt number given by Eq. (6) is calculated to be 1.05, indicating a nearly perfect separability of the BWF.

2. Maximally Polarization Entangled Photons

We now consider the generation of maximally polarization entangled photons, which requires zero GVM between the downconverted photons. This could not be satisfied in Fig. 3 even if the waveguide width further decreases beyond ~2.5 μm, as the modes are cut off due to weak confinement in the vertical direction. Alternatively, one could adjust the core thickness to achieve zero GVM between the downconverted photons. The group velocities of the downconverted modes as functions of the core thickness are shown in Fig. 5, for a waveguide width of 3 μm, while keeping all other parameters unchanged from before. The core thickness for zero GVM is found to be 529 nm, with a corresponding QPM grating period of 2.98 μm. The required core thickness is also a function of waveguide width, as shown in Fig. 6. Zero GVM between the downconverted modes could not be achieved if the waveguide width is smaller than 2.5 μm due to the increased form birefringence.

Notice that $Al_xGa_{1-x}As$ is nonbirefringent, which allows for zero GVM between the downconverted photons in weakly guided waveguides. In birefringent materials, however, strong confinement is necessary to achieve this in general.

To characterize the quality of polarization entanglement, we take the example of $W = 3$ μm and $t_c = 529$ nm, and assume the pump is narrow band, i.e., $|\phi(\omega)|^2 \approx \delta(\omega - \omega_p)$. For a 2 mm long waveguide, the spectral intensities $|\Phi_{\alpha\beta}(\omega_1, \omega_2)|^2$ and the associated phases are shown in Fig. 7,

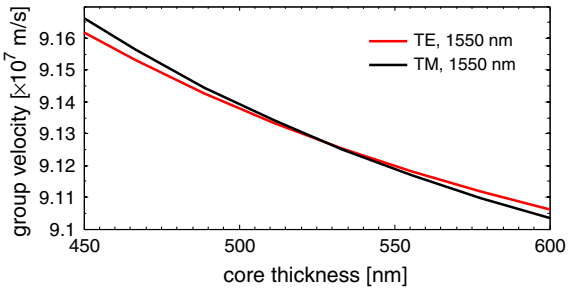

Fig. 5. Group velocities of the downconverted modes as functions of the core thickness, for an Al_xGa_{1-x} As waveguide with a width of 3 μm.

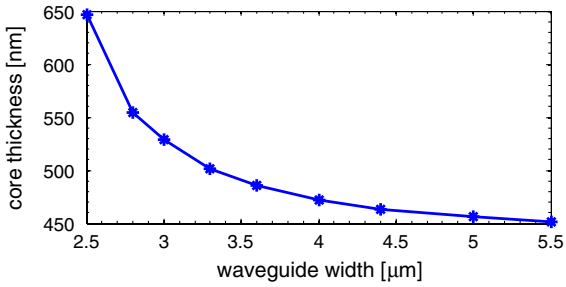

Fig. 6. Dependence of the core thickness on the waveguide width that satisfies zero GVM between the downconverted modes for an Al_xGa_{1-x} As waveguide.

after integrating over ω_2. The two polarizations show almost identical spectra and phases, making it impossible to discern the polarization of a photon without polarization measurements. The concurrence C given by Eq. (10) is calculated to be almost unity, with $1 - C \approx 6.1 \times 10^{-5}$. This confirms that the polarization entanglement is nearly maximal.

B. Ferroelectric Waveguides

To demonstrate that the technique of two-photon quantum state engineering using dispersion engineering in photonic nanowire waveguides is not limited to a particular material system, we consider the waveguide designs using ferroelectric material lithium niobate, which is commonly used in wavelength conversion and photon pair generation. Lithium niobate waveguides with large index contrast can be fabricated by techniques such as crystal ion slicing and wafer bonding [44]. In the following discussions, we assume z-cut periodically poled lithium niobate (PPLN) is bonded to a silica lower cladding layer, and the waveguide length is 10 mm. The structure is schematically shown in Fig. 2(b). Cross-polarized photons can be generated via a type-II process with a TE polarized pump. We will now follow the same procedure to discuss the generation of pure single photons and maximally polarization entangled photons.

1. Pure Single Photons

Taking a core thickness of 1 μm, the dependences of the group velocities on the waveguide width are shown in Fig. 8. Notice that due to a smaller material dispersion than that of $Al_xGa_{1-x}As$, group velocity matching required by Eq. (5)

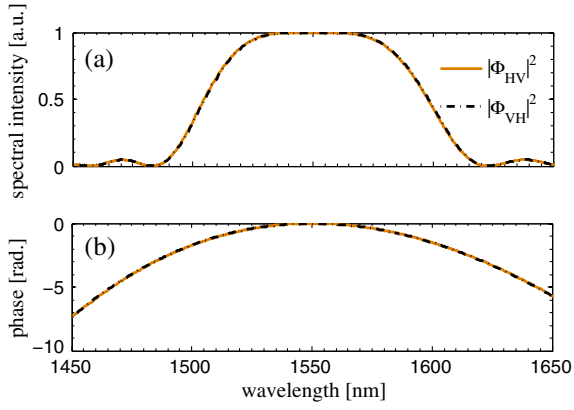

Fig. 7. (a) Spectral intensities and (b) corresponding phases of the downconverted photons generated in an Al_xGa_{1-x} As waveguide with a core thickness of 529 nm and width $W = 3$ μm using a CW pump.

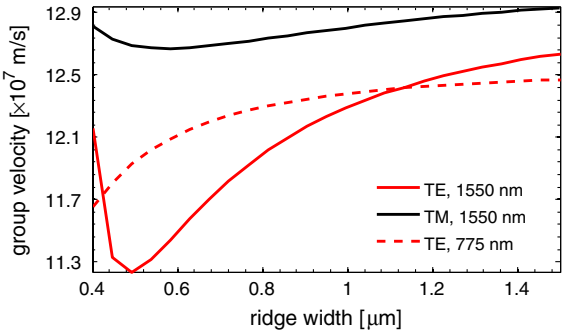

Fig. 8. Dependences of group velocities on the width for a PPLN waveguide with a core thickness of 1 μm.

can be more easily satisfied in lithium niobate. Figure 8 shows that group velocity matching can be satisfied in a large range of 0.42 μm≤$W \leq$ 1.12 μm. In particular, when $W \approx 1.12$ μm with a corresponding QPM grating period of 3.49 μm, $v_H^d = v_H^p$, and uncorrelated photons with different spectra can be generated with a pump sufficiently broad. The JSI generated by 200 fs pump pulses is shown in Fig. 9(a), with the corresponding Schmidt number calculated to be 1.05.

An interesting feature of this design is that uncorrelated photons with almost identical spectra can be generated when the width $W \approx 0.71$ μm, which satisfies $2/v_H^p = 1/v_H^d + 1/v_V^d$. In this case, the QPM grating period is 2.63 μm. For a waveguide length of 10 mm, the optimal pump pulse duration is found to be 1.7 ps, which results in a Schmidt number of 1.18. The corresponding JSI is shown in Fig. 9(b). Moreover, as mentioned before, switching between correlated, uncorrelated, and anticorrelated photon pairs can be simply achieved by varying the pump pulse duration.

2. Maximally Polarization Entangled Photons

Achieving zero GVM between the cross-polarized downconverted photons in PPLN waveguides is somewhat different from that in $Al_xGa_{1-x}As$ waveguides. In the latter case, as we have shown, the lack of material birefringence makes it possible to achieve zero GVM in weakly guided waveguides, whereas in PPLN, significant GVM due to material birefringence has to be canceled in strongly confined waveguides with large index contrast, as illustrated in Fig. 2(b).

In Fig. 8, we observe that $v_V^d > v_H^d$ regardless of the waveguide width when the core thickness is 1 μm. Following our discussion in Section 3, with a large index contrast in the vertical direction, v_V^d can be decreased by decreasing the core

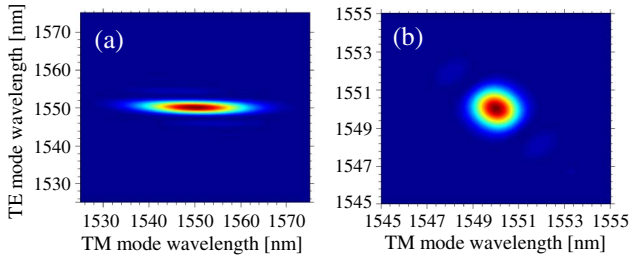

Fig. 9. Joint spectral intensities of the generated photon pairs in a PPLN waveguide with a core thickness of 1 μm (a) using 200 fs pump pulses when $W \approx 1.12$ μm, and (b) using 1.7 ps pump pulses when $W \approx 0.71$ μm. The corresponding Schmidt numbers are 1.05 and 1.18, respectively.

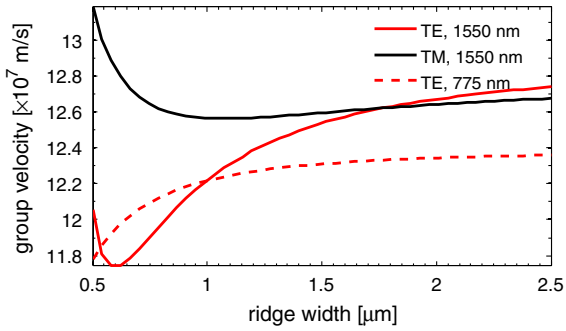

Fig. 10. Dependences of group velocities on the width for a PPLN waveguide with a core thickness of 0.5 μm.

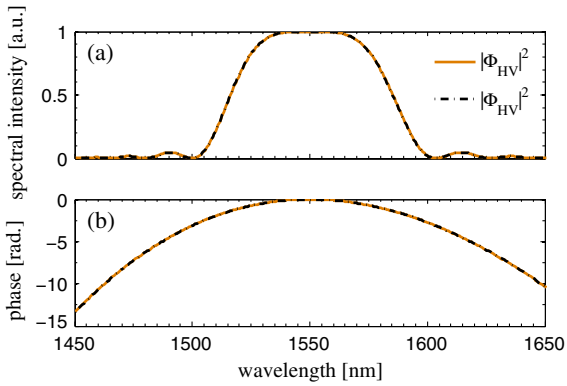

Fig. 11. (a) Spectral intensities and (b) corresponding phases of the downconverted photons generated in a PPLN waveguide with a core thickness of 0.5 μm and width $W = 1.76$ μm using a CW pump.

thickness. We therefore decrease the core thickness to 0.5 μm, and calculate the group velocities as functions of the waveguide width, as shown in Fig. 10. The result shows that $v_V^d = v_H^d$ can indeed be satisfied when the width $W = 1.76$ μm. The corresponding QPM grating period is 2.32 μm. Of course the required waveguide width is also a function of the core thickness. In this case, the downconverted photons again show almost identical spectra and phases, as shown in Fig. 11. The calculated concurrence C satisfies $1 - C \approx 6.0 \times 10^{-6}$, indicating a maximal polarization entanglement. Notice that uncorrelated photons with different spectra can also be generated in the range of 0.53 μm$\leq W \leq$ 1.00 μm.

5. DISCUSSION AND CONCLUSION

In this work, we have developed a strategy to achieve two-photon quantum state engineering for photon pairs generated via SPDC in nonlinear waveguides with subwavelength confinement. By varying the waveguide dimension, the group velocity of each mode involved in the SPDC process can be tuned, which allows for group velocity matching for either the pump and one of the downconverted photons, or the two downconverted photons in pairs. This makes it possible to generate pure heralded single photons, or maximally polarization entangled photons directly from the chip.

We further applied this method to III–V semiconductor Al_xGa_{1-x} As waveguides and ferroelectric lithium niobate waveguides. The results show that heralded single photons with a Schmidt number close to unity and polarization entangled photons with a concurrence of one can be generated in both material systems. We must emphasize that this technique of two-photon quantum state engineering could be applied to $\chi^{(2)}$ nonlinear waveguides of any material system in principle, and could generate the desired quantum state not naturally allowed by material dispersions.

Fabrication of the waveguides designed in this work is challenging due to their small characteristic dimensions and the strict requirements on the roughness, which greatly impacts the attainable propagation losses. However, most of the crucial steps for these devices have been developed already. For $Al_xGa_{1-x}As$, tightly confined nanowire ridge waveguides with high aspect ratios exceeding 10 and ridge widths less than 300 nm have been demonstrated by several groups [28,45]. QPM in $Al_xGa_{1-x}As$ is not trivial but has been demonstrated using several techniques such as orientation patterning [46] and quantum well intermixing [47]. On the other hand, lithium niobate thin film and ridge waveguides [44,48,49], as well high index contrast nanowires with cross-section areas <1 μm [50], have been developed, driven by a whole range of applications including the enhanced wavelength conversion efficiency and electro-optic modulation. Second-harmonic generation using QPM with third-order gratings in PPLN nanowires has been demonstrated with the fundamental wavelength of 1064 nm [50]. Meanwhile, short period QPM gratings as small as 400 nm have been developed for PPLN [51,52].

It must be noted that, for photonic nanowires, in which waveguide dispersion dominates over material dispersion, fabrication imperfection may cause significant deviation from the waveguide design parameters and hence reduce the quality of the generated state. Considering the PPLN designs corresponding to Figs. 9(a) and 11 for example, a change of the grating period by 0.5% can shift the QPM wavelength of the photon pairs by ~50 nm, increasing the Schmidt number to 1.83 under the same pump pulse duration and decreasing the concurrence to 0.22, respectively. On the other hand, if the waveguide widths are changed by 1%, the Schmidt number will increase to 1.90, while the concurrence will decrease to 0.57.

Such low tolerances require careful optimization on the fabrication processes. Nevertheless, one can use third-order QPM gratings to ease the tolerance requirement and design the waveguide dimensions such that group velocity matching can be safely satisfied even with considerable fabrication errors. Single photons with Schmidt numbers close to 1 can thus be generated by choosing the right combination of the waveguide length and pump duration. For polarization entanglement, one can apply weak bandpass filtering to increase the concurrence. For the state with a concurrence of 0.22 mentioned above, a 10 nm bandpass filter can increase the concurrence to 0.96 without any off-chip compensation. Note that such a filtering bandwidth is one order of magnitude more relaxed than the bandwidth of typical type-II SPDC in PPLN weakly guided waveguides and such filters can be implemented on the same chip.

The devices designed in this work are generally robust to temperature fluctuations. For a temperature fluctuation as large as 20°C, both $Al_xGa_{1-x}As$ and PPLN waveguides have a shift of QPM wavelength of within 10 nm for the downconverted photons. This results in an enhancement of the Schmidt number by less than 0.06 for both material systems,

and reduction of the concurrences to 0.97 for $Al_xGa_{1-x}As$ and 0.70 for PPLN. On the other hand, temperature control can be easily deployed to partially compensate for any fabrication errors.

Lastly, we note that the technique described in this work is compatible with the recent development of integrated quantum photonics [3,53,54]. Combined with other components such as on-chip interferometry circuits and detectors, this technique provides a viable route to achieve fully integrated generation and manipulations of photonic quantum qubits.

ACKNOWLEDGMENTS

The authors thank N. Zareian and R. Marchildon for helpful comments. This work was supported by the Natural Sciences and Engineering Research Council of Canada (NSERC).

REFERENCES

1. N. Gisin, G. Ribordy, W. Tittel, and H. Zbinden, "Quantum cryptography," Rev. Mod. Phys. **74**, 145–195 (2002).
2. T. D. Ladd, F. Jelezko, R. Laflamme, Y. Nakamura, C. Monroe, and J. L. O'Brien, "Quantum computers," Nature **464**, 45–53 (2010).
3. J. L. O'Brien, A. Furusawa, and J. Vučković, "Photonic quantum technologies," Nat. Photonics **3**, 687–695 (2009).
4. E. Bimbard, N. Jain, A. MacRae, and A. I. Lvovsky, "Quantum-optical state engineering up to the two-photon level," Nat. Photonics **4**, 243–247 (2010).
5. J. P. Torres, K. Banaszek, and I. A. Walmsley, "Engineering nonlinear optic sources of photonic entanglement," Prog. Opt. **56**, 227–331 (2011).
6. K. Edamatsu, "Entangled photons: generation, observation, and characterization," Jpn. J. Appl. Phys. **46**, 7175–7187 (2007).
7. Y. H. Kim, S. P. Kulik, and Y. Shih, "Bell-state preparation using pulsed nondegenerate two-photon entanglement," Phys. Rev. A **63**, 060301(R) (2001).
8. T. Kim, M. Fiorentino, and F. N. C. Wong, "Phase-stable source of polarization-entangled photons using a polarization Sagnac interferometer," Phys. Rev. A **73**, 012316 (2006).
9. M. D. Eisaman, J. Fan, A. Migdall, and S. V. Polyakov, "Invited review article: single-photon sources and detectors," Rev. Sci. Instrum. **82**, 071101 (2011).
10. N. Mizuochi, T. Makino, H. Kato, D. Takeuchi, M. Ogura, H. Okushi, M. Nothaft, P. Neumann, A. Gali, F. Jelezko, J. Wrachtrup, and S. Yamasaki, "Electrically driven single-photon source at room temperature in diamond," Nat. Photonics **6**, 299–303 (2012).
11. A. Christ, A. Fedrizzi, H. Hübel, T. Jennewein, and C. Silberhorn, "Parametric down-conversion," Exper. Methods Phys. Sci. **45**, 351–410 (2013).
12. W. P. Grice, A. B. U'Ren, and I. A. Walmsley, "Eliminating frequency and space-time correlations in multiphoton states," Phys. Rev. A **64**, 063815 (2001).
13. T. Suhara, "Generation of quantum-entangled twin photons by waveguide nonlinear-optic devices," Laser Photon. Rev. **3**, 370–393 (2009).
14. G. Fujii, N. Namekata, M. Motoya, S. Kurimura, and S. Inoue, "Bright narrowband source of photon pairs at optical telecommunication wavelengths using a type-II periodically poled lithium niobate waveguide," Opt. Express **15**, 12769–12776 (2007).
15. J. Chen, A. J. Pearlman, A. Ling, J. Fan, and A. Migdall, "A versatile waveguide source of photon pairs for chip-scale quantum information processing," Opt. Express **17**, 6727–6740 (2009).
16. R. Horn, P. Abolghasem, B. J. Bijlani, D. Kang, A. S. Helmy, and G. Weihs, "Monolithic source of photon pair," Phys. Rev. Lett. **108**, 153605 (2012).
17. J. G. Rarity, J. Fulconis, J. Duligall, W. J. Wadsworth, and P. St. J. Russell, "Photonic crystal fiber source of correlated photon pairs," Opt. Express **13**, 534–544 (2005).
18. J. Fan, A. Migdall, and L. J. Wang, "Efficient generation of correlated photon pairs in a microstructure fiber," Opt. Lett. **30**, 3368–3370 (2005).
19. C. Xiong, L. G. Helt, A. C. Judge, G. D. Marshall, M. J. Steel, J. E. Sipe, and B. J. Eggleton, "Quantum-correlated photon pair generation in chalcogenide As_2S_3 waveguides," Opt. Express **18**, 16206–16216 (2010).
20. N. Lv, W. Zhang, Y. Guo, Q. Zhou, Y. Huang, and J. Peng, "1.5 μm polarization entanglement generation based on birefringence in silicon wire waveguides," Opt. Lett. **38**, 2873–2876 (2013).
21. A. Eckstein, A. Christ, P. J. Mosley, and Ch. Silberhorn, "Highly efficient single-pass source of pulsed single-mode twin beams of light," Phys. Rev. Lett. **106**, 013603 (2011).
22. J. Svozilík, M. Hendrych, A. S. Helmy, and J. P. Torres, "Generation of paired photons in a quantum separable state in Bragg reflection waveguides," Opt. Express **19**, 3115–3123 (2011).
23. D. Kang and A. S. Helmy, "Generation of polarization entangled photons using concurrent type-I and type-0 processes in AlGaAs ridge waveguides," Opt. Lett. **37**, 1481–1483 (2012).
24. S. V. Zhukovsky, L. G. Helt, D. Kang, P. Abolghasem, A. S. Helmy, and J. E. Sipe, "Generation of maximally-polarization-entangled photons on a chip," Phys. Rev. A **85**, 013838 (2012).
25. D. Kang, L. G. Helt, S. V. Zhukovsky, J. P. Torres, J. E. Sipe, and A. S. Helmy, "Hyperentangled photon sources in semiconductor waveguides," Phys. Rev. A **89**, 023833 (2014).
26. S. M. Spillane, M. Fiorentino, and R. G. Beausoleil, "Spontaneous parametric down conversion in a nanophotonic waveguide," Opt. Express **15**, 8770–8780 (2007).
27. M. A. Foster, A. C. Turner, J. E. Sharping, B. S. Schmidt, M. Lipson, and A. L. Gaeta, "Broad-band optical parametric gain on a silicon photonic chip," Nature **441**, 960–963 (2006).
28. D. Duchesne, K. A. Rutkowska, M. Volatier, F. Légaré, S. Delprat, M. Chaker, D. Modotto, A. Locatelli, C. De Angelis, M. Sorel, D. N. Christodoulides, G. Salamo, R. Arès, V. Aimez, and R. Morandotti, "Second harmonic generation in AlGaAs photonic wires using low power continuous wave light," Opt. Express **19**, 12408–12417 (2011).
29. P. Abolghasem, M. Hendrych, X. Shi, J. P. Torres, and A. S. Helmy, "Bandwidth control of paired photons generated in monolithic Bragg reection waveguides," Opt. Lett. **34**, 2000–2002 (2009).
30. K. Garay-Palmett, H. J. McGuinness, O. Cohen, J. S. Lundeen, R. Rangel-Rojo, A. B. U'Ren, M. G. Raymer, C. J. McKinstrie, S. Radic, and I. A. Walmsley, "Photon pair-state preparation with tailored spectral properties by spontaneous four-wave mixing in photonic-crystal fiber," Opt. Express **15**, 14870–14886 (2007).
31. M. Halder, J. Fulconis, B. Cemlyn, A. Clark, C. Xiong, W. J. Wadsworth, and J. G. Rarity, "Nonclassical 2-photon interference with separate intrinsically narrowband fibre sources," Opt. Express **17**, 4670–4676 (2009).
32. S. Azzini, D. Grassani, M. J. Strain, M. Sorel, L. G. Helt, J. E. Sipe, M. Liscidini, M. Galli, and D. Bajoni, "Ultra-low power generation of twin photons in a compact silicon ring resonator," Opt. Express **20**, 23100–23107 (2012).
33. R. Kumar, J. R. Ong, J. Recchio, K. Srinivasan, and S. Mookherjea, "Spectrally multiplexed and tunable-wavelength photon pairs at 1.55 μm from a silicon coupled-resonator optical waveguide," Opt. Lett. **38**, 2969–2971 (2013).
34. N. Matsuda, H. L. Jeannic, H. Fukuda, T. Tsuchizawa, W. J. Munro, K. Shimizu, K. Yamada, Y. Tokura, and H. Takesue, "A monolithically integrated polarization entangled photon pair source on a silicon chip," Sci. Rep. **2**, 817 (2012).
35. L. Olislager, J. Safioui, S. Clemmen, K. P. Huy, W. Bogaerts, R. Baets, P. Emplit, and S. Massar, "Silicon-on-insulator integrated source of polarization-entangled photons," Opt. Lett. **38**, 1960–1962 (2013).
36. W. P. Grice and I. A. Walmsley, "Spectral information and distinguishability in type-II down-conversion with a broadband pump," Phys. Rev. A **56**, 1627–1634 (1997).
37. Z. Yang, M. Liscidini, and J. E. Sipe, "Spontaneous parametric down-conversion in waveguides: a backward Heisenberg picture approach," Phys. Rev. A **77**, 033808 (2008).

38. L. G. Helt, E. Y. Zhu, M. Liscidini, L. Qian, and J. E. Sipe, "Proposal for in-fiber generation of telecom-band polarization-entangled photon pairs using a periodically poled fiber," Opt. Lett. **34**, 2138–2140 (2009).
39. M. M. Fejer, G. A. Magel, D. H. Jundt, and R. L. Byer, "Quasi-phase-matched second harmonic generation: tuning and tolerances," IEEE J. Quantum Electron. **28**, 2631–2654 (1992).
40. S. Hill and W. K. Wootters, "Entanglement of a pair of quantum bits," Phys. Rev. Lett. **78**, 5022–5025 (1997).
41. W. K. Wootters, "Entanglement of formation of an arbitrary state of two qubits," Phys. Rev. Lett. **80**, 2245–2248 (1998).
42. S. Gehrsitz, F. K. Reinhart, C. Gourgon, N. Herres, A. Vonlanthen, and H. Sigg, "The refractive index of $Al_xGa_{1-x}As$ below the band gap: accurate determination and empirical modeling," J. Appl. Phys. **87**, 7825–7837 (2000).
43. G. E. Edwards and M. Lawrence, "A temperature-dependent dispersion equation for congruently grown lithium niobate," Opt. Quantum Electron. **16**, 373–375 (1984).
44. P. Rabiei and W. H. Steier, "Lithium niobate ridge waveguides and modulators fabricated using smart guide," Appl. Phys. Lett. **86**, 161115 (2005).
45. J. Meier, W. S. Mohammed, A. Jugessur, L. Qian, M. Mojahedi, and J. S. Aitchison, "Group velocity inversion in AlGaAs nanowires," Opt. Express **15**, 12755–12762 (2007).
46. K. A. Fedorova, A. D. McRobbie, G. S. Sokolovskii, P. G. Schunemann, and E. U. Rafailov, "Second harmonic generation in a low-loss orientation-patterned GaAs waveguide," Opt. Express **21**, 16424–16430 (2013).
47. A. S. Helmy, D. C. Hutchings, T. C. Kleckner, J. H. Marsh, A. C. Bryce, J. M. Arnold, C. R. Stanley, J. S. Aitchison, C. T. A. Brown, K. Moutzouris, and M. Ebrahimzadeh, "Quasi phase matching in GaAs-AlAs superlattice waveguides through bandgap tuning by use of quantum-well intermixing," Opt. Lett. **25**, 1370–1372 (2000).
48. D. Djukic, G. Cerda-Pons, R. M. Roth, R. M. Osgood, S. Bakhru, and H. Bakhru, "Electro-optically tunable second-harmonic-generation gratings in ion-exfoliated thin films of periodically poled lithium niobate," Appl. Phys. Lett. **90**, 171116 (2007).
49. H. Lu, B. Sadani, N. Courjal, G. Ulliac, N. Smith, V. Stenger, M. Collet, F. I. Baida, and M.-P. Bernal, "Enhanced electro-optical lithium niobate photonic crystal wire waveguide on a smart-cut thin film," Opt. Express **20**, 2974–2981 (2012).
50. G. Poberaj, H. Hu, W. Sohler, and P. Günter, "Lithium niobate on insulator (LNOI) for micro-photonic devices," Laser Photonics Rev. **6**, 488–503 (2012).
51. A. C. Busacca, C. L. Sones, V. Apostolopoulos, R. W. Eason, and S. Mailis, "Surface domain engineering in congruent lithium niobate single crystals: a route to submicron periodic poling," Appl. Phys. Lett. **81**, 4946–4948 (2002).
52. A. Busacca, M. Cherchi, S. R. Sanseverino, A. C. Cino, A. Parisi, G. Assanto, M. Cichoki, F. Caccavale, D. Calleyo, and A. Morbiato, "Surface periodic poling in lithium niobate and lithium tantalate," in *Proceedings of 2005 IEEE/LEOS Workshop on Fibres and Optical Passive Components* (IEEE, 2005), pp. 126–130.
53. L. Sansoni, F. Sciarrino, G. Vallone, P. Mataloni, A. Crespi, R. Ramponi, and R. Osellame, "Two-particle Bosonic-Fermionic quantum walk via integrated photonics," Phys. Rev. Lett. **108**, 010502 (2012).
54. A. Gaggero, S. Jahanmiri Nejad, F. Marsili, F. Mattioli, R. Leoni, D. Bitauld, D. Sahin, G. J. Hamhuis, R. Nötzel, R. Sanjines, and A. Fiore, "Nanowire superconducting single-photon detectors on GaAs for integrated quantum photonic applications," Appl. Phys. Lett. **97**, 151108 (2010).